Available online at www.sciencedirect.com
SCIENCE DIRECT®
Journal of Solid State Chemistry 178 (2005) 3040–3045
JOURNAL OF SOLID STATE CHEMISTRY
www.elsevier.com/locate/jssc

Hydrothermal synthesis and structure characterization of a new 3D vanadium hydrogen phosphite with 14-ring channels: $(C_5N_2H_{14})[VO(H_2O)]_3(HPO_3)_4 \cdot H_2O$

Ray-Kuang Chiang*, Niang-Tsu Chuang

Department of Chemical Engineering, Far East College, Tainan County 74448, Taiwan, Republic of China

Received 25 April 2005; received in revised form 23 May 2005; accepted 24 May 2005

Abstract

A new 3D vanadium hydrogen phosphite, $(C_5N_2H_{14})[VO(H_2O)]_3(HPO_3)_4 \cdot H_2O$, has been prepared by hydrothermal reactions and characterized by single crystal X-ray diffraction, infrared spectroscopy, thermogravimetric analysis, and magnetic techniques. It crystallizes in the triclinic space group $P\text{-}1$ (no. 2) with $a = 6.258(1)$ Å, $b = 9.696(2)$ Å, $c = 19.384(4)$ Å, $\alpha = 76.124(3)^\circ$, $\beta = 83.726(4)^o$, $\gamma = 75.222(4)^o$, $Z = 2$. The structure is built up from sharing equatorial oxygen atoms of $VO_5(H_2O)$ octahedra with HPO_3 tetrahedra, which can be viewed as a (3,4) connected net. The framework is mainly constructed by two types of four-ring related chains. Intrachain and interchain hydrogen bonds play an important role on supporting the framework structure. The 14-ring tunnels in the structure are filled with 1-methypiperazinium and water molecules, which also contribute the hydrogen bonding with the vanadium phosphite framework.

Keywords: Vanadium phosphite

1. Introduction

The four-connected aluminum silicates and aluminum phosphates comprise a large number of microporous compounds based on the tunable framework charges originated from the different Al/Si (or Al/P) ratios and the effects of structure-directing agents [1]. Transition metal phosphates provide more variables with respect to their predecessor not only in valence states but also in geometric shapes and connecting modes [2]. It is manifest from the above reasons that the structure variety of vanadium phosphates and organophosphonates is plenty, since the oxidation state of vanadium may vary among 3, 4, and 5, and the coordination polyhedron of vanadium may vary among tetrahedron, square pyramid, trigonal bipyramid, and octahedron [3]. Furthermore, the flexibility of coordination and oxidation state are beneficial to some practical applications such as coordination intercalation and catalyst [4,5]. Thus, the research of vanadium phosphate has been very extensive [6–12]. Recently, research interest is also aroused in replacing four-connected PO_4 units with three-connected HPO_3 units to expand the structure variety of the polyhedron-based frameworks. Organically templated transition metal phosphites with interesting structure diversity, such as V, [13–19] Cr, [14,20] Mn, [21,22] Fe, [23–25] Co, [26] and Zn [27–45] phosphites, have been reported. In our studies of the effects of organic templates on the structural chemistry of open-framework structures, a 1-methylpiperazinium templated oxovanadium phosphite with 14-ring channels was synthesized. In this paper, we report its synthesis, structure, and some physical properties.

*Corresponding author. Fax: 886 6 597 7767.
E-mail address: rkc.chem.@msa.hinet.net (R.-K. Chiang).

0022-4596/$ - see front matter © 2005 Published by Elsevier Inc.
doi:10.1016/j.jssc.2005.05.040

2. Experimental

2.1. Synthesis and characterization of $(C_5N_2H_{14})[VO(H_2O)]_3(HPO_3)_4 \cdot H_2O$

A pure phase of **1** in the form of light blue plate-like crystals can be prepared from a reaction mixture of 0.5 mmole V_2O_3 (99%, Aldrich), 5 mmole H_3PO_3 (98%, Acros), 0.1 mmole 1-methylpiperazine (99%, Acros), and 8.0 mL distilled water heated in a hydrothermal reactor at 160 °C for 48 h under autogeneous pressure. The yield is 43% based on 1-methylepiperazine. At less acidic condition the known phase of $[VO(H_2O)](HPO_3)$ is always present in the product. The reaction condition involved oxidation of V(III) to V(IV). Chemical analysis confirmed the amount of diprotonated 1-methylepiperazine in the structure (Found: C, 8.55; H, 3.44; N, 3.93. Cald: C, 8.64; H, 3.77; N, 4.03.). Thermogravimetric analysis was carried out in nitrogen at a heating rate of 10 °C/min (Perkin Elmer Instruments, TGA 7). Magnetic susceptibility was measured under 5000 Oe from 3 to 300 K (SQUID, Quantum Design).

2.2. Structure determination

A crystal of dimension $0.50 \times 0.30 \times 0.10$ mm was glued on a glass fiber and mounted on a smart CCD diffractometer using Mo K_α radiation. Intensity data were collected for indexing in 2070 frames with increasing ω (width of 0.3° per frame). Of the 5456 reflections collected ($2\theta_{max} = 56.7°$), 4877 reflections were considered observed ($I_{obs} > 2\sigma(I)$) after Lp and absorption corrections. The absorption correction was based on symmetry-equivalent reflections using the *SADABS* programs [46]. On the basis of systematic absences and statistic intensity distribution, the space group was determined to be *P*-1. Direct methods were used to first locate the V atoms and the P atoms, and the remaining oxygen, carbon, and nitrogen atoms were found from successive difference maps. All H atoms were located on difference Fourier maps calculated at the final stage of structure refinement. The final cycles of refinement, including the atom coordinates and anisotropic thermal parameters for all nonhydrogen atoms and fixed atomic coordinates and isotropic thermal parameters for the hydrogen atoms, converged at $R_1 = 0.0452$ and $wR_2 = 0.1319$. In the final difference map the deepest hole was $-0.93\,e\,Å^{-3}$ and the highest peak was $1.13\,e\,Å^{-3}$. Anomalous and secondary extinction correction were applied. All calculations were performed by using the *SHELXTL* programs [47]. The crystallographic data are summarized in Table 1.

Table 1
Crystallographic data for **1**

	1
Formula	$C_5N_2H_{26}V_3P_4O_{19}$
Crystal system	Triclinic
Space group	*P*-1
Fw	694.98
Cell dimensions	$a = 6.258(1)$ Å, $\alpha = 76.124(3)°$ $b = 9.696(2)$ Å, $\beta = 83.726(4)°$ $c = 19.384(4)$ Å, $\gamma = 75.222(4)°$
Volume	1102.6(4) Å^3
Z	2
Temp	294(2)
λ (Å)	0.71073
ρ_{calcd} (g cm^{-3})	2.093
μ (cm^{-1})	16.27
R indices[a] [$I > 2\sigma(I)$]	$R_1 = 0.0452$, $wR_2 = 0.1319$
R indices [all data]	$R_1 = 0.0492$, $wR_2 = 0.1392$

[a] $R_1 = \Sigma\|F_o| - |F_c\|/\Sigma|F_o|$,
$wR_2 = [\Sigma w(|F_o|^2 - |F_c|^2)^2/\Sigma w(|F_o|^2)^2]^{1/2}$,
$w = [\sigma^2 F_o^2 + 0.0703P]^2 + 0.6368P]$, where $P = (F_o^2 + 2F_c^2)/3$.

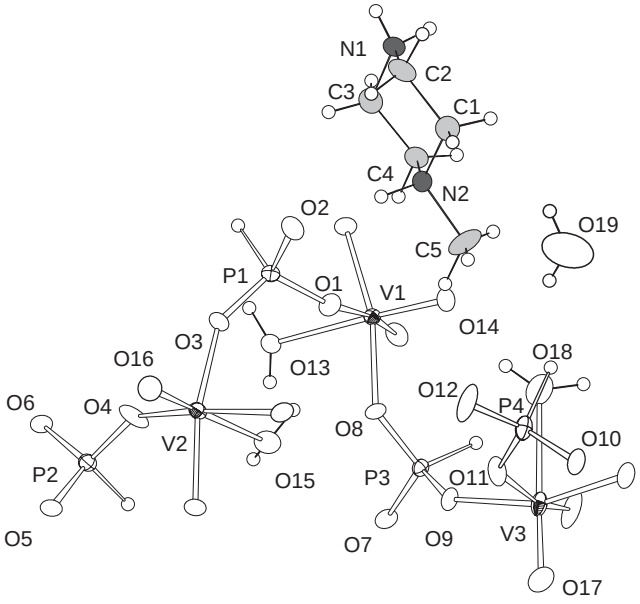

Fig. 1. Asymmetric unit of **1** showing the connection of V and P polyhedra: thermal ellipsoids are shown at 50% probability.

3. Results and Discussion

3.1. Structure of $(C_5N_2H_{14})[VO(H_2O)]_3(HPO_3)_4 \cdot H_2O$

The 3D framework structure of compound **1** is built by the corner-sharing $VO_5(H_2O)$ octahedra and HPO_3 tetrahedra. It contains three unique vanadium atoms and four unique phosphorus atoms (Fig. 1). All the V atoms in **1** are tetravalent (bond valence sums [48] listed in Table 2), and adopt a 1+4+1 octahedral

environment with one short, four intermediate, and one long V–O bond distances. The short V–O distances are in the range of 1.603(2)–1.619(2) Å indicating the vanadyl groups present. The four oxygen atoms with intermediate VO distances are in the range of 1.965(2)–2.026(2) Å, which are the bridging oxygen shared with HPO_3 tetrahedra. The long V–O distances in the range of 2.236(2)–2.414(4) Å are attributed to water molecules with a weak coordination to the vanadium atoms. The 3D structure may be viewed as complex V–P–O layers linked through the double chains consisting of V(3) and P(4) (type-A) into a pillared motif with 14-polyhedra channels (Fig. 2). This type-A chain is built by edged-fused 4-ring through -1 symmetry at the center of the 4-ring resulted in alternatively corner-shared $VO_5(H_2O)$ octahedra and HPO_3 tetrahedra (Fig. 3a). The water molecules attached to V(3) are in a weaker manner than those attached to V(1) and V(2) based on the longer bond distances (Table 2). These water molecules and pairs of unbonded water molecules occupied at the center of the channels, and pairs of diprotonated 1-methylpiperazine cations are situated in two envelopes of the oval-shaped channels. Within the complex V–P–O layer, we further dissected out another type of chain (type-B) consisting of V(1), P(1), V(2), and P(3). These chains are also four-ring related but with only one-side covalently linked; the other side is supported by hydrogen bonds (Fig. 3b). Hydrogen bonds play an important role on supporting the

Table 2
Selected bond lengths (Å) and bond valence sums for **1**

V(1)–O(14)	1.619(2)	V(1)–O(1)	2.006(2)
V(1)–O(2)	2.022(2)	V(1)–O(6)	1.999(2)
V(1)–O(8)	1.988(2)	V(1)–O(13)	2.236(2)
$\sum s$(V(1)–O) = 3.97			
V(2)–O(16)	1.603(2)	V(2)–O(3)	2.015(2)
V(2)–O(5)	1.995(2)	V(2)–O(4)	1.988(2)
V(2)–O(7)	2.026(2)	V(2)–O(15)	2.266(2)
$\sum s$(V(2)–O) = 4.00			
V(3)–O(17)	1.618(3)	V(3)–O(9)	1.993(2)
V(3)–O(10)	1.969(2)	V(3)–O(11)	2.006(2)
V(3)–O(12)	1.965(2)	V(3)–O(18)	2.414(5)
$\sum s$(V(3)–O) = 3.99			
P(1)–O(1)	1.520(2)	P(1)–O(2)	1.532(2)
P(1)–O(3)	1.519(2)	P(2)–O(4)	1.515(2)
P(2)–O(5)	1.517(2)	P(2)–O(6)	1.525(2)
P(3)–O(7)	1.521(2)	P(3)–O(8)	1.519(2)
P(3)–O(9)	1.527(2)	P(4)–O(10)	1.525(2)
P(4)–O(11)	1.522(2)	P(4)–O(12)	1.514(2)
N(1)–C(2)	1.483(5)	N(1)–C(3)	1.496(4)
N(2)–C(1)	1.494(4)	N(2)–C(4)	1.497(4)
N(2)–C(5)	1.491(5)	C(1)–C(2)	1.517(5)
C(3–C(4)	1.504(5)		

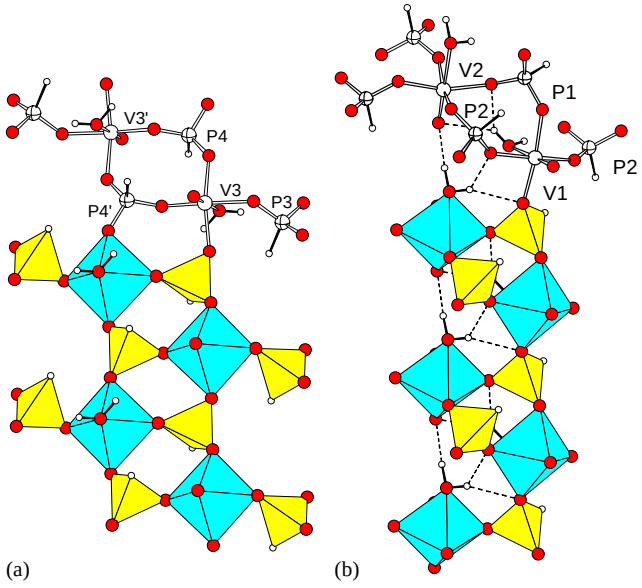

Fig. 3. Structure construction units of **1**: (a) type-A chains with alternatively corner-shared $VO_5(H_2O)$ octahedra and HPO_3 tetrahedra in an edge-fused fashion, (b) type-B chain four-ring relayed with one-side covalently linked.

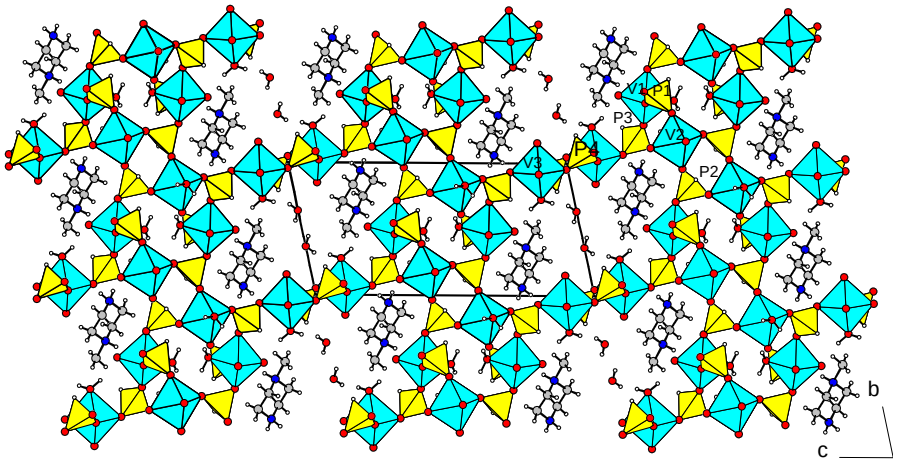

Fig. 2. Polyhedral view of **1** showing the 14-ring tunnels along the [100] direction.

Table 3
Hydrogen bonds for **1** (Å/deg)

D-H···A	*d*(H···A)	*d*(H···A)	*d*(D···A)	∠DHA
N1-H1C···O7	0.844	2.158	2.882	143.76
N1-H1C···O15	0.844	2.267	2.886	130.31
N1-H1D···O9	0.952	2.133	2.966	145.46
N1-H1D···O11	0.952	2.281	3.003	132.12
N2-H2C···O2	0.950	1.936	2.844	159.10
N2-H2C···O14	0.950	2.361	3.007	124.86
O13-H13A···O3	0.910	2.104	2.857	139.45
O13-H13A···O16	0.910	2.366	3.114	139.49
O13-H13B···O4	0.991	1.833	2.751	152.41
O13-H13B···O3	0.991	2.488	3.126	121.86
O15-H15A···O8	0.882	2.136	2.771	128.30
O15-H15A···O1	0.882	2.248	3.067	154.29
O15-H15B···O16	1.067	1.846	2.885	163.41
O18-H18A···O14	0.954	1.939	2.884	170.17
O18-H18B···O19	1.019	1.776	2.758	160.51
O19-H19A···O19	0.826	2.144	2.895	151.17

structure in **1** including intrachain (type-B), interchain (between type-A and type-B), and amine to framework types (Table 3). Each P(2) moiety in the layer is further interlinked via its three oxygen atoms with three different chains of type-B to form a thick layer generating six-ring and four-ring channels along the *a*-axis and 10-ring channels along the *c*-axis. Alternatively, the complex V–P–O layer can be viewed as center symmetry related double sheets, in which type-B chains are interlinked through P(2) pyramids to form a 2D structure with 10-ring openings.

It is interesting to relate the structure construction units in **1** to known vanadium phosphates and phosphites. Both the type-A and type-B chains in **1** consist of four-ring units, which are very common in vanadium phosphates. The ladder-like type-A chain is reminiscent of the 1D structure of $VO(HPO_4)\cdot 4H_2O$, which can be viewed as a geometrical fragment in the layer structures of α-$VOPO_4$ and $VO(HPO_4)\cdot 2H_2O$. [49,50] However, this is not surprising that the extending restriction is not prominent for the phosphite moiety to mimic the phosphate moiety in low-dimensional structures. A similar topology as in type-A chain is also found in the 1D structure of $(C_2H_{10}N_2)[M(HPO_3)F_3]$ (M = V(III) and Cr(III)) [15]. For 2D and 3D structures the difference should gradually appear, because the 3-connected phosphite unit is different from the 4-connected phosphate unit, especially considering the charge difference between $(HP^{III}O_3)^{2-}$ and $(P^{V}O_4)^{3-}$. For instance, the layered $(H_2ppz)[(VO)_3(HPO_3)_4(H_2O)]$ structure [13] is different from any known structures of diprotonated pipperazine templated vanadium phosphates [51]. Although the above description is a legitimate assumption, interesting exceptions may exit. For example, 3D $(CN_3H_6)\cdot Zn(HPO_3)_2$ is structurally similar to its phosphate analogue, $(CN_3H_6)\cdot Zn(HPO_4)_2$, in which $(HPO_3)^{2-}$ and $(HPO_4)^{2-}$ can be viewed as equivalent species [30]. This is probably ascribed to the insignificant PO-H···O hydrogen bonds in $(CN_3H_6)\cdot Zn(HPO_4)_2$. These examples display complexities in the interesting and unpredictable transition metal phosphate systems.

3.2. Thermogravimetric analysis

The thermogravimetric analysis of **1** showed several continuous weight losses (Fig. 4). The first one between 30 and 110 °C (5.4%) and the second one between 110 to 260 °C (5.2%) are attributed to the removal of the four water molecules in **1** (calc. 10.4%). The O(18) water molecules with long V–O bonds to V(3) pointing toward the 14-ring channels are reasonable to be removed easilier than those attached to V(1) and V(2). Therefore, the weight loss in the first stage is attributed to the removal of O(19) (interstitial water) and O(18), and the second stage is attributed to the removal of O(13) and O(15). The removal of water in stage 1 will leave the structure with free space at the center of the 1D channel. To test its sorption ability, a sample of **1** heated at 120 °C for 5 min was cooled down on a balance in air. Interestingly, the weight increased immediately to its original value with the structure remained. This phenomenon is ascribed to its re-absorption of water from the air. The structure sustains up to 200 °C, and this suggests **1** may be useful as sorbents via the vacant coordination site on V(3) after its coordination water expelled. The amine leaves the structure after 260 °C with the destruction of the structure. The weight loss was continued till 900 °C with 76% weight remained. After 900 °C some weight increased. The residual of the TGA experiment, identified by powder X-ray, appears to be a mixture of $(VO)_2(P_4O_{12})$ (JCPDS 34-1040) and $H_{7.24}V_6O_{13}$ (JCPDS 37-0172).

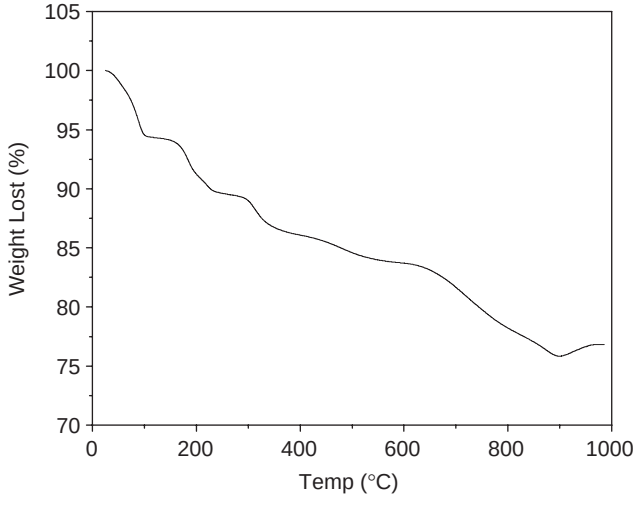

Fig. 4. Thermogravimetric analysis for **1**.

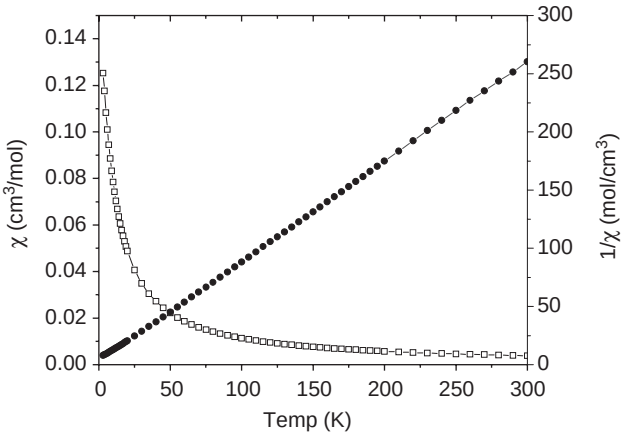

Fig. 5. Temperature-dependent magnetic susceptibility data for **1**; χ vs. T and χ^{-1} vs. T.

3.3. Magnetic susceptibility

The variable temperature magnetic susceptibility for **1** is shown in Fig. 5. The linear behavior of $1/\chi$(T) above 25 K obeys well the Curie–Weiss equation ($C = 1.16\,\mathrm{cm^3\,K/mol}$, $\theta = -2.24\,\mathrm{K}$). The effective magnetic moment per metal atom at 300 K, $1.78\,\mu_B$, is consistent with the spin-only value of V(IV) ($1.73\,\mu_B$). This is also in agreement with the results from BVS calculation.

Acknowledgments

We thank the National Science Council (NSC 92-2113-269-001) and Far East College for support, and Prof. S.L. Wang and Ms. F.-L. Liao at National Tsing Hua University for X-ray intensity data collection.

References

[1] J. Yu, R. Xu, Acc. Chem. Res. 36 (2003) 481.
[2] A.K. Cheetham, G. Ferey, T. Loiseau, Angew. Chem. Int. Ed. 38 (1999) 3268.
[3] S. Boudin, A. Guesdon, A. Leclaire, M.-M. Borel, Int. J. Inorg. Mater. 2 (2000) 561.
[4] G.W. Coulston, S.R. Bare, H. Kung, K. Birkeland, G.K. Bethke, R. Harlow, N. Herron, P.L. Lee, Science 275 (1997) 191.
[5] J.W. Johnson, A.J. Jacobson, W.M. Butler, S.E. Rosenthal, J.F. Brody, J.T. Lewandowski, J. Am. Chem. Soc. 111 (1989) 381.
[6] V. Soghomonian, Q. Chen, R.C. Haushalter, J. Zubieta, C.J. O'Connor, Science 259 (1993) 1596.
[7] V. Soghomonian, Q. Chen, R.C. Haushalter, J. Zubieta, Angew. Chem. Int. Ed. 32 (1993) 610.
[8] V. Soghomonian, Q. Chen, R.C. Haushalter, J. Zubieta, Chem. Mater. 5 (1993) 1595.
[9] V. Soghomonian, Q. Chen, R.C. Haushalter, J. Zubieta, C.J. O'Connor, Y.S. Lee, Chem. Mater. 5 (1993) 1690.
[10] T. Loiseau, G. Ferey, J. Solid State Chem. 111 (1994) 416.
[11] V. Soghomonian, R.C. Haushalter, Q. Chen, J. Zubieta, Inorg. Chem. 33 (1994) 1700.
[12] X. Bu, P. Feng, G.D. Stucky, J. Chem. Soc. Chem. Commun. (1995) 1337.
[13] G. Bonavia, J. DeBord, R.C. Haushalter, D. Rose, J. Zubieta, Chem. Mater. 7 (1995) 1995.
[14] S. Fernandez, J.L. Mesa, J.L. Pizarro, L. Lezama, M.I. Arriortua, T. Rojo, Chem. Mater. 14 (2002) 2300.
[15] S. Fernandez, J.L. Mesa, J.L. Pizarro, L. Lezama, M.I. Arriortua, T. Rojo, Chem. Mater. 15 (2003) 1204.
[16] W.T.A. Harrison, Issue Series Title: Solid State Sci. 5 (2003) 297.
[17] Z. Shi, D. Zhang, G. Li, L. Wang, X. Lu, J. Hua, S. Feng, J. Solid State Chem. 172 (2003) 464.
[18] Z. Shi, G. Li, D. Zhang, J. Hua, S. Feng, Inorg. Chem. 42 (2003) 2357.
[19] S. Shi, L. Wang, H. Yuan, G. Li, J. Xu, G. Zhu, T. Song, S. Qiu, J. Solid State Chem. 177 (2004) 4183.
[20] S. Fernandez, J.L. Mesa, J.L. Pizarro, L. Lezama, M.I. Arriortua, T. Rojo, Angew. Chem. Int. Ed. 41 (2002) 3683.
[21] S. Fernandez, J.L. Mesa, J.L. Pizarro, L. Lezama, M.I. Arriortua, R. Olazcuaga, T. Rojo, Chem. Mater. 12 (2000) 2092.
[22] S. Fernandez, J.L. Pizarro, J.L. Mesa, L. Lezama, M.I. Arriortua, R. Olazcuaga, T. Rojo, Inorg. Chem. 40 (2001) 3476.
[23] S. Fernandez, J.L. Mesa, J.L. Pizarro, L. Lezama, M.I. Arriortua, T. Rojo, Chem. Mater. 14 (2002) 2300.
[24] S. Fernandez-Armas, J.L. Mesa, J.L. Pizarro, J.S. Garitaonandia, M.I. Arriortua, T. Rojo, Angew. Chem. Int. Ed. 43 (2004) 977.
[25] U.-C. Chung, J.L. Mesa, J.L. Pizarro, L. Lezama, J.S. Garitaonandia, J.P. Chapman, M.I. Arriortua, J. Solid State Chem. 177 (2004) 2705.
[26] S. Fernandez, J.L. Pizarro, J.L. Mesa, L. Lezama, M.I. Arriortua, T. Rojo, Int. J. Inorg. Mater. 3 (2001) 331.
[27] J.A. Rodgers, W.T.A. Harrison, Chem. Commun. 23 (2000) 2385.
[28] W.T.A. Harrison, M.L.F. Phillips, J. Stanchfield, T.M. Nenoff, Inorg. Chem. 40 (2001) 895.
[29] W.T.A. Harrison, J. Solid State Chem. 160 (2001) 4.
[30] W.T.A. Harrison, M.L.F. Phillips, J. Chem. Soc. Dalton Trans. (2001) 2459.
[31] M.L.F. Phillips, T.M. Nenoff, C.T. Thompson, W.T.A. Harrison, J. Solid State Chem. 167 (2002) 337.
[32] J.-H. Liao, P.-L. Chen, C.-C. Hsu, J. Phys. Chem. Solids 62 (2001) 1629.
[33] W. Dong, G. Li, Z. Shi, W. Fu, D. Zhang, X. Chen, Z. Dai, L. Wang, S. Feng, Inorg. Chem. Commun. 6 (2003) 776.
[34] Y. Wang, J. Yu, Y. Du, Z. Shi, Y. Zou, R. Xu, J. Chem. Soc. Dalton Trans. (2002) 4060.
[35] J. Liang, Y. Wang, J. Yu, Y. Li, R. Xu, Chem. Commun. (2003) 882.
[36] W.T.A. Harrison, R.M. Yeates, M.L.F. Phillips, T.M. Nenoff, Inorg. Chem. 42 (2003) 1493.
[37] Y. Wang, J. Yu, Y. Li, Y. Du, R. Xu, L. Ye, J. Solid State Chem. 170 (2003) 303.
[38] Z.-E. Lin, J. Zhang, S.-T. Zheng, Q.-H. Wei, G.-Y. Yang, Solid State Sci. 5 (2003) 1435.
[39] L.E. Gordon, W.T.A. Harrison, Inorg. Chem. 43 (6) (2004) 1808.
[40] S. Suhua, Q. Wei, L. Guanghua, W. Li, Y. Hongming, X. Jianing, Z. Guangshan, S. Tianyou, Q. Shilun, J. Solid State Chem. 177 (2004) 3038.
[41] D. Zhang, Z. Shi, W. Dong, W. Fu, L. Wang, G. Li, S. Feng, J. Solid State Chem. 177 (2004) 343.
[42] J.-X. Pan, S.-T. Zheng, G.-Y. Yang, Microporous Mesoporous Mater. 75 (2004) 129.
[43] Z.-E. Lin, J. Zhang, S.-T. Zheng, G.-Y. Yang, Microporous Mesoporous Mater. 68 (2004) 65.
[44] A. Kirkpatrick, W.T.A. Harrison, Solid State Sci. 6 (2004) 593.

[45] J. Fan, C. Slebodnick, D. Troya, R. Angel, B.E. Hanson, Inorg. Chem. 44 (2005) 2719.
[46] G.M. Sheldrick, SADABS, Program for Siemens Area Detector Absorption Corrections, University of Gottingen, Germany, 1997.
[47] G.M. Sheldrick, SHELXTL Programs, Version 5.1, Bruker AXS GmbH, Karlsruhe, Germany, 1998.
[48] I.D. Brown, D. Altermatt, Acta Crystallogr. B 41 (1985) 244.
[49] Y.-M. Tsai, S.-L. Wang, C.-H. Huang, K.-H. Lii, Inorg. Chem. 38 (1999) 4183.
[50] M.E. Leonowicz, J.W. Johnson, J.F. Brody, H.F. Shannon, J.M. Newsam, J. Solid State Chem. 56 (1985) 370.
[51] J. Do, R.P. Bontchev, A.J. Jacobson, J. Solid State Chem. 154 (2000) 514.